Radiation Measurements xxx (2010) 1–12

Contents lists available at ScienceDirect

Radiation Measurements

journal homepage: www.elsevier.com/locate/radmeas

Decomposition of the angular ESR spectra of fossil tooth enamel fragments

Renaud Joannes-Boyau*, Thomas Bodin, Rainer Grün

Research School of Earth Sciences, The Australian National University, Canberra, ACT 0200, Australia

ARTICLE INFO

Article history:
Received 25 June 2009
Received in revised form
25 May 2010
Accepted 11 June 2010

Keywords:
ESR dating
Fossil tooth enamel
CO_2-radicals

ABSTRACT

The ESR spectra of a fragment of fossil tooth enamel were measured by rotating it in 10° increments over 360° around its three major axes. We used an automated simulated annealing (SA) procedure for the mathematical decomposition of the spectra. The SA approach is particularly robust in finding global solutions rather than getting stuck in local minima. All angular measurements could be fitted with four Gaussian lines, all of which could be attributed to components of CO_2^- radicals. The results imply that the tooth enamel fragment contains at least two different types of oriented CO_2^- radicals, plus about 9% of non-oriented CO_2^- radicals. The oriented components were tentatively attributed to axial and orthorhombic CO_2^- radicals. Their explicit locations in the crystal domains of the tooth enamel remain unresolved.

1. Introduction

To minimize the impact of the analysis on important archaeological samples, non-destructive ESR analysis has been carried out on tooth enamel fragments rather than powders (Grün, 2006). Nevertheless, the use of fragments for dose reconstruction has strongly complicated the task due to the high anisotropy of tooth enamel crystal. Grün et al. (2008) showed that the angular irradiation response of fragments is different to that of powders due to the presence of at least two different types of CO_2^- radicals (oriented and non-oriented). The non-oriented CO_2^- radicals (NOCORs) give rise to a powder spectrum of the same intensity at all angles, while the intensities of the anisotropic CO_2^- radicals (AICORs) are angular dependent. Because of different relative distributions and thermal stabilities of these two types of CO_2^- radicals in the natural and irradiated spectrum components, the calculated dose values become angular dependent.

AICORs may occur in two varieties: axial CO_2^- radicals (with $g_\perp$ around 1.9925 and $g_\parallel$ around 1.9974, e.g. Callens et al., 1987; Ishchenko et al., 2002) occur through carbonate substitution of the PO_4^{3-} tetrahedron (e.g. Vugman et al., 1995). Their axial symmetry is explained by rotation around the O–O axis which is in direction of the mineralogical *c*-axis of the hydroxyapatite crystals. Orthorhombic CO_2^- radicals (with g_x, g_z and g_y around 2.0030, 2.0015 and 1.9973, respectively, e.g. Callens et al., 1987; Ishchenko et al., 2002; Rudko et al., 2007) are associated with carbonate substitution of $(OH)^-$. Their explicit location is disputed. Some speculated that they are located at the surface of the hydroxyapatite crystals (Callens et al., 1995; Brik et al., 2000, 2005), while others argued them to be in the same position as the axial CO_2^- radicals (Ishchenko et al., 2002; Vorona et al., 2005).

At specific angles, when the g_x, g_z or $g_\perp$ of the AICORs are largest (T1–B1 dominant, Fig. 1), the $g_y/g_\parallel$ components, which correspond to the B2 dip (Fig. 1C), are mainly composed by NOCORs. Using these specific positions, the fitting of a powder spectrum (obtained by merging all angles of configurations) into the spectra allows the estimation of the amount of NOCORs in the sample. The NOCORs are then subtracted at every angle. Nonetheless, some B_2 component of the AICORs may also be removed with the subtraction of the NOCORs. One has to keep in mind that the T1–B1 peak may consist of a range of radicals (methyl, CO_3^{3-}, CO^-, CO_3^- etc., for a compilation see Callens et al., 1998; Vanhaelewyn et al., 2000b). Only CO_2^- radicals, which may occur as orthorhombic, axial or non-oriented types, have any signal intensity in the B2 region through their g_y or $g_\parallel$ components. Tumbling CO_2^- radicals give rise of an isotropic line at $g = 2.0006 \pm 0.0001$ (Callens et al., 1987; Debuyst et al., 1993; Vanhaelewyn et al., 2000b; Vorona et al., 2006).

Thus far, all papers dealing with the description and interpretation of the ESR spectra of enamel fragments focussed only on specific angles, particularly when the peaks in the T1–B1 and B2 positions were largest or smallest. The spectra recorded for intermediate angles were usually not further discussed. However, these are important for validating proclaimed interpretations. For example, we found that it was not possible to fit intermediate spectra of irradiated fossil tooth enamel with a linear combination of the natural signal and a NOCOR powder spectrum. This means that there are more than just two radicals involved in the natural and/or irradiated spectra of fossil tooth enamel. This was already

* Corresponding author. Tel.: +61 261253122.
E-mail address: renaud.joannes-boyau@anu.edu.au (R. Joannes-Boyau).

1350-4487/$ – see front matter © 2010 Elsevier Ltd. All rights reserved.
doi:10.1016/j.radmeas.2010.06.029

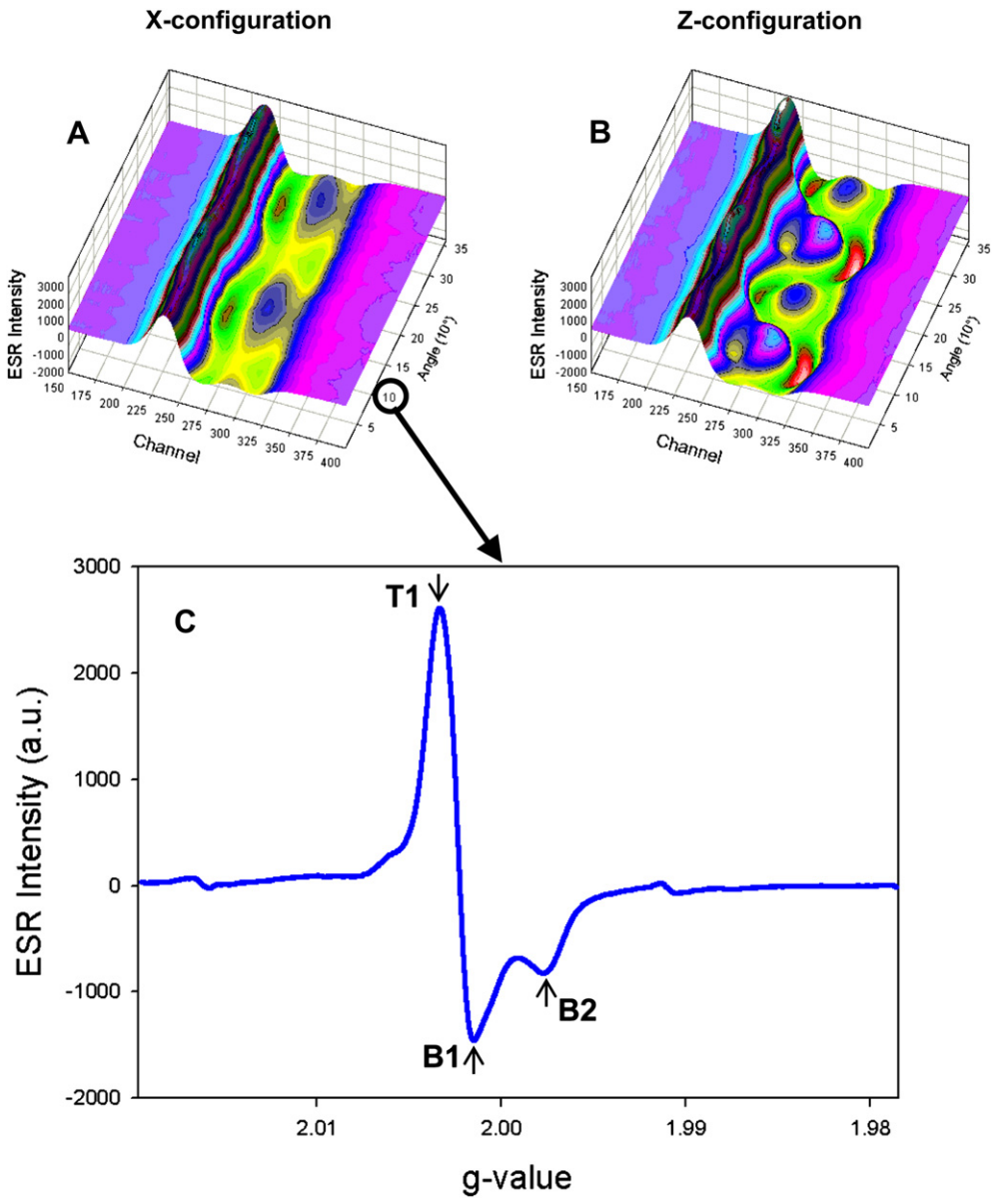

Fig. 1. Stacked ESR spectra of X- and Z-configuration (A,B) and indication of the major spectrum positions (C).

pointed out in the heating experiments by Joannes-Boyau and Grün (2009). In this paper, we present the decomposition of all ESR spectra of a fossil tooth enamel fragment that was rotated around its three major axes in 10° increments.

2. Materials and methods

In this paper X, Y and Z denote configurations, *x*, *y* and *z* the main axes of the measured fragment (Fig. 2). T1, B1 and B2 are positions in the measured or simulated ESR spectra (Fig. 1), R_1, R_2, R_3 and B_2 fitted Gaussian components (Fig. 4).

The experiments were carried out on a tooth enamel fragment of a fossil bovid from the archaeological site of Holon (Porat et al., 1999). A long lamella was separated from the tooth using a dentist's diamond saw and series of consecutive fragments were cut and used for a range of heating and irradiation experiments (e.g. Grün et al., 2008; Joannes-Boyau and Grün, 2009).

The fragment (H5) was successively mounted into three separate Teflon holders containing Parafilm moulds. This allowed for the rotation of the fragment around its three major axes along with the incremental measurements of ESR spectra. We used the following configurations: X: rotation around the axis perpendicular to the dentine–enamel junction, Y: around the axis of tooth growth and Z: perpendicular to X and Y (Fig. 2). The sample holders were inserted in a Bruker ER 218PG1 programmable goniometer and measured with a Bruker Elexys E500 ESR spectrometer in 10° increments over 360° with the following measurement conditions: 2 mW microwave power, 0.1 mT modulation amplitude 12 mT sweep width with a sweep time of 21 s. The spectra were accumulated from 50 consecutive measurements.

All spectrum decompositions and simulations were carried out on the measured derivative spectra. Initially we used the Matlab software with the easyspin add-on (Stoll and Schweiger, 2006, 2007). For simplification, only line shapes defined by the first derivative of the Gaussian function were used, although there were indications that in some cases Lorentzian or Voigtian line shapes were perhaps more appropriate. Some apparent signals in the residual (measured minus simulated) spectra seemed to be due to

Please cite this article in press as: Joannes-Boyau, R., et al., Decomposition of the angular ESR spectra of fossil tooth enamel fragments, Radiation Measurements (2010), doi:10.1016/j.radmeas.2010.06.029

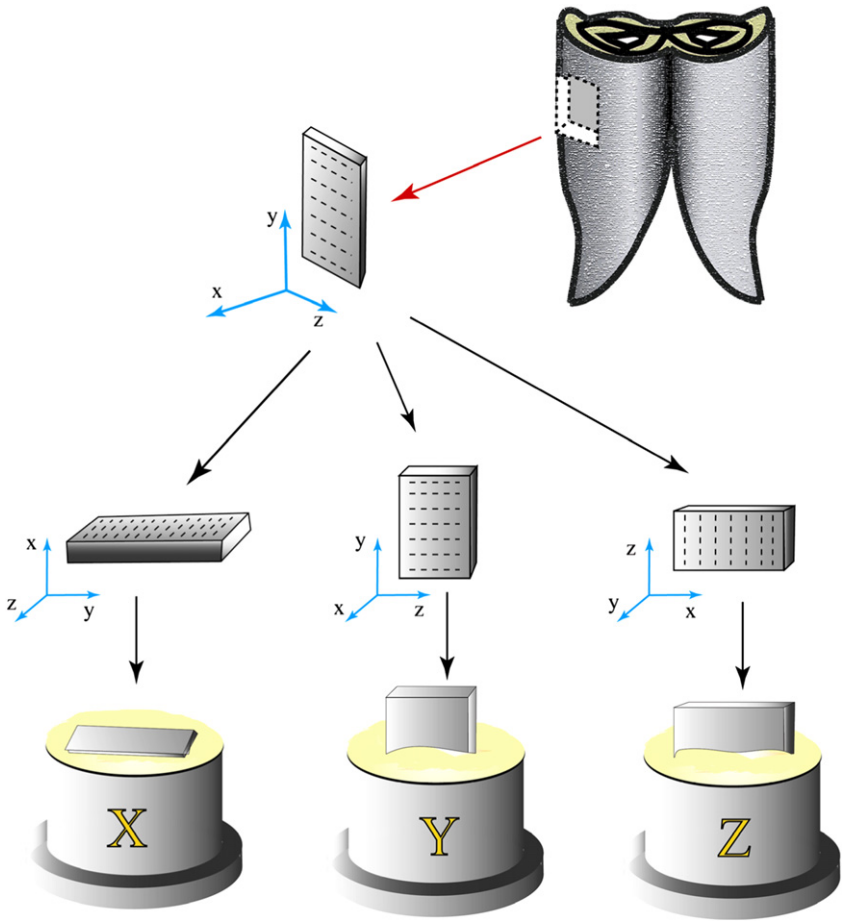

Fig. 2. Direction of axes and configurations used for the measurement of the tooth enamel fragment.

the error induced by the Gaussian approximation. After several subjective manual approaches to spectrum analysis, decomposition was optimised and automated using a simulated annealing (SA) procedure. SA is a Monte Carlo method used for combinatorial optimisation problems (for details see Metropolis et al., 1953; Kirkpatrick et al., 1983; Černý, 1985; Mosegaard and Sambridge, 2002). Our SA procedure is able to randomly generate a large number of synthetic spectra defined by a linear combination of four Gaussian lines. Each simulated spectra is compared to the measured spectra in terms of a least square misfit. The particular advantage of the SA algorithm is the search of the global minimum misfit without getting stuck in local solutions. As we shall see below, SA can resolve completely overlapping signals, which are very difficult to decompose with alternative decomposition approaches.

The Gaussian lines had prescribed limits with respect to the *g*-value range to avoid unrealistic solutions outside the regions for the CO_2^- radical in hydroxyapatite (see above). No restrictions were set on the intensity and maximum line width, however, a minimum width (0.10 mT) was defined to avoid aberrations.

3. Results and discussion

ESR spectra of fragments differ from those of powders due to the pronounced anisotropy of the CO_2^- radical (e.g. Fig. 1). The angular variations of the ESR spectra vary from one configuration to the other. The anisotropy of the measured spectra of the Z-configuration (Fig. 1B, Table 2) is significantly larger than of the other two configurations. The X-configuration shows the smallest anisotropic effects (Fig. 1A), while the Y-configuration appears to show a mixed pattern of the other two.

3.1. Spectrum decomposition

When a single orthorhombic crystal is rotated around the *y* or *z* axis, a signal will appear at different *g*-values, shifting from the parallel (g_z, g_x) to the perpendicular position (g_y), as shown in Fig. 3. In contrast, enamel fragments are a partially ordered system and mostly only minor *g*-value shifts have been observed for the T1–B1 and B2 components. This could be the result of a combination of interfering oriented and non-oriented radicals or multiple orientations of the main CO_2^- radical. Spectrum decomposition should help the understanding of the behaviour of known radicals that are supposedly involved in the spectra.

The ESR spectra of tooth enamel have a range of non-CO_2^- components, such as dimethyl radicals. To subtract these, a merged spectrum was produced (the average of all measured spectra). In the range used for decomposition, the measured spectra contain a dimethyl triplet and two wide lines (Fig. 4A). W1, around $g = 2.0061$, was also described by Grün (2002) but could not be attributed to a specific radical. W2, around $g = 2.0051$, relates most likely to a combination of SO_2^- and CO^- radicals which occur at $g = 2.0056$ and $g = 2.0047$, respectively (Bouchez et al., 1988; Schramm and Rossi, 2000, see also the fitting of Grün, 2002, his Fig. 1G and H). The intensity of the central dimethyl line was derived from the next two outer lines assuming a septet with

Please cite this article in press as: Joannes-Boyau, R., et al., Decomposition of the angular ESR spectra of fossil tooth enamel fragments, Radiation Measurements (2010), doi:10.1016/j.radmeas.2010.06.029

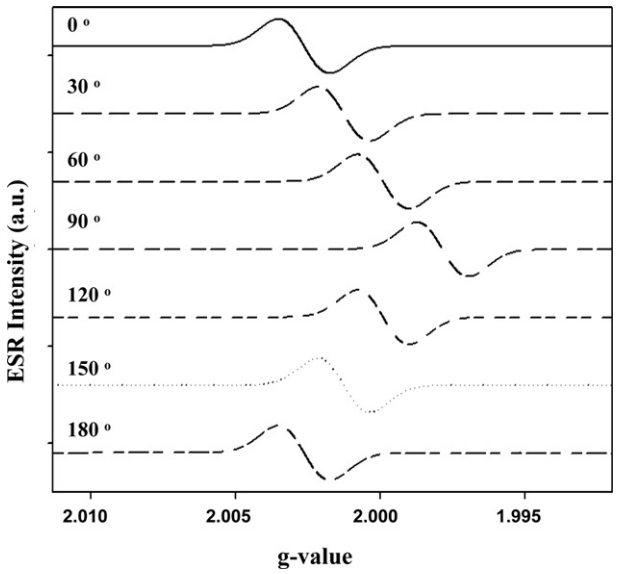

Fig. 3. Simulated angular ESR spectra of orthorhombic CO_2^- radicals in a single hydroxyapatite crystal with the mineralogical *c*-axis in the rotation plane.

intensity distribution of a Pascal triangle. None of these components exhibited any quantifiable angular variation, thus they were assumed to be isotropic. The two wide lines were combined with the dimethyl lines into an iso-combined (IC) spectrum (Fig. 4A) which has an intensity of about 25% of the merged spectrum (Fig. 4A). However, most of the IC intensity lies outside the range of CO_2^- radicals and will have little effect on the decomposition results. The IC spectrum was subtracted from all angular measurements.

While the X-configuration can be reasonably fitted with just three components (R_1, R_2, and B_2, see Fig. 4B), the Y- and Z-configurations require an additional component (R_3) to obtain a satisfactory match between experimental spectrum and simulation. The introduction of R_3 resulted in a division of the original B_2 signal that was abnormally wide and intense (compare the fitting results in Fig. 4B and C). In this context we prefer the use of B_2 rather than R_4, since all our previous papers uses B2 for the dip around $g = 1.9976$ (see also Fig. 1C).

At this stage, we did not subtract a NOCOR component from the measured spectra, as this does not have an influence on the angular behaviour of the various components (it only causes constant offsets). In the first instance, its maximum intensity can be derived from the minimum B2 position in X-configuration and cannot exceed 13% of the total radical concentration.

3.2. Decomposition of the spectra of the three configurations

The description of the results starts with the Z-configuration, which showed the largest angular changes. The radical concentrations were derived from the double integration of the fitted lines to account for changes in the line width (Table 2 and Figs. 5I, 6I and 7I). The angular variation is expressed in the difference between maximum and minimum concentration divided by the average concentration of the fitted component $(C_{max} - C_{min})/C_{av}$. For features in the measured ESR spectra, T1–B1 and B2, it was not possible to carry out double integrations, their angular variations were derived from their intensities (Table 1). The results for the various fitted components are listed in Table 2.

3.2.1. Z-configuration

The Z-configuration shows the largest angular dependency of the measured spectra between the T1–B1 maximum and the B2 maximum 90° later (see Fig. 5A, H and I), with large angular variations in the T1–B1 and B2 intensities of 0.60 and 0.74, respectively. Fig. 5 shows the results of the fitting. Generally, there is a very good match between the measured and fitted spectra (Fig. 5A–C, top row). The intensities in the residual stack (measured minus fitted spectrum, Fig. 5C) are well below 5% of the measured spectra (Fig. 5A). The results on the individual components are shown in the rows below.

As expected from the measured spectra, B_2 shows the largest radical concentrations (0.55) of all configurations and large angular variations (0.54, see Fig. 5H,I). In contrast to the behaviour in the

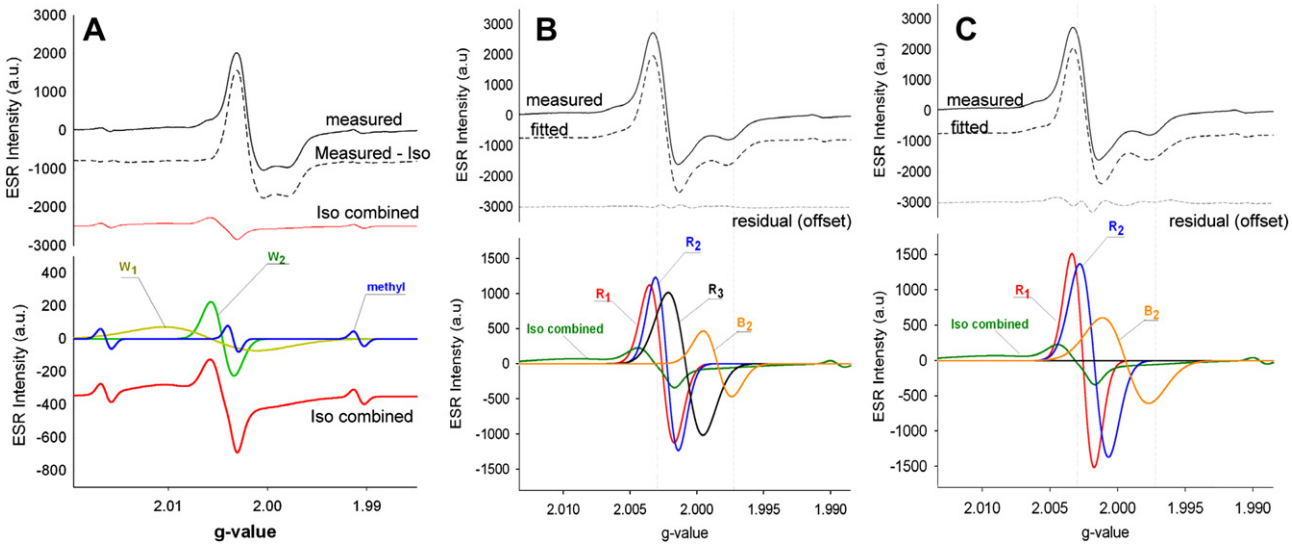

Fig. 4. Decomposition of the measured spectra. A (Top): Comparison of the measured and simulated spectra. The residual is offset for better understanding and corresponds to the subtraction of the simulated spectra from the measured. (Bottom): Position of the isotropic lines which were combined and subtracted from all measured spectra. B: (Top): Comparison of the measured and simulated spectra. The residual is offset for better understanding and corresponds to the subtraction of the simulated spectra from the measured (Bottom): Decomposition using four Gaussian components. C: (Top): Comparison of the measured and simulated spectra. The residual is offset for better understanding and corresponds to the subtraction of the simulated spectra from the measured (Bottom) Decomposition using three Gaussian components.

Please cite this article in press as: Joannes-Boyau, R., et al., Decomposition of the angular ESR spectra of fossil tooth enamel fragments, Radiation Measurements (2010), doi:10.1016/j.radmeas.2010.06.029

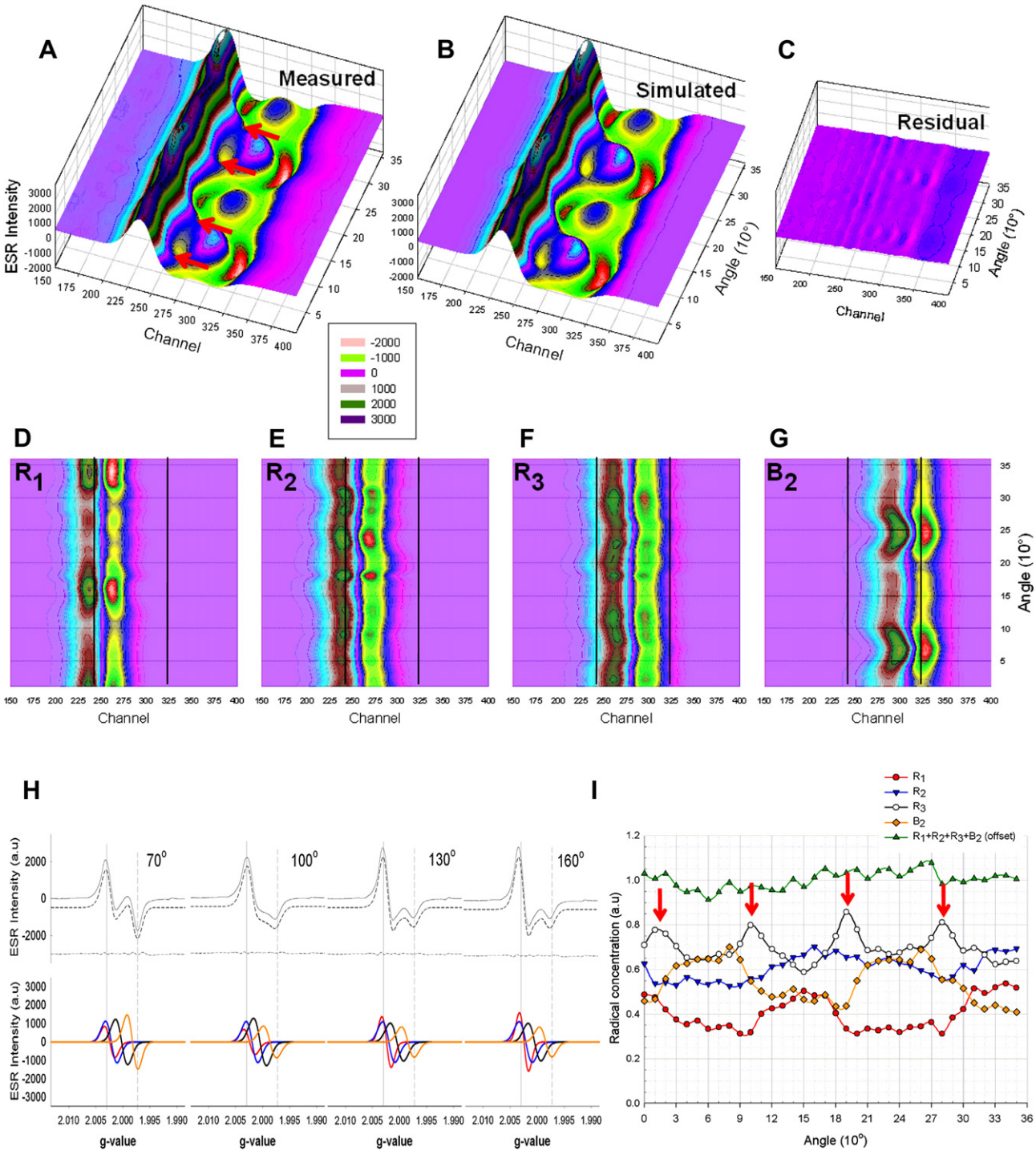

Fig. 5. Decomposition of the spectra in Z-configuration. A: 3D view of measured spectra. The arrows indicate widening of the T1–B2 complex which is due to R_3 (see Fig. 5H). B: 3D view of simulated spectra. C: 3D view of residual (measured minus simulated). D–G: Intensity maps of Gaussian components R1, R2, R3 and B2. The scale is the same as in A–C. The lines indicate the position of $g = 2.0030$ (solid line) and $g = 1.9975$ (dotted). H: decomposition of selected spectra (starting angle where T1–B2 intensity is maximum, over 90° with 30° steps) with lines indicating $g = 2.0030$ and $g = 1.9975$. I: Summary of all decomposition results. Note that D–I show ESR intensities while H shows radical concentrations (obtained by double integration). These take into account changes in line width. R3 shows a 90° symmetry (arrows).

other configurations, B_2 changes its line width (between 0.33 and 0.42 mT) and *g*-value (between 1.9981 and 1.9987) considerably (see Fig. 5G and Table 2). This has some influence on the calculation of the B_2 concentrations. As a result, the angular variability of the B_2 component is somewhat smaller than expected from the intensity changes in the B2 position.

R_1 and R_2 show very similar angular behaviours, with their maxima and minima offset from B_2 by about 90°. The main intensity changes in T1–B1 (0.60) are due to the angular response of R_1 (0.56) while R_2 shows significantly less angular variation (0.29). Similar to B_2, the line width of R_1 changes significantly (0.28 to 0.36 mT), but its *g*-value remains within a narrow range (2.0025–2.0027).

Please cite this article in press as: Joannes-Boyau, R., et al., Decomposition of the angular ESR spectra of fossil tooth enamel fragments, Radiation Measurements (2010), doi:10.1016/j.radmeas.2010.06.029

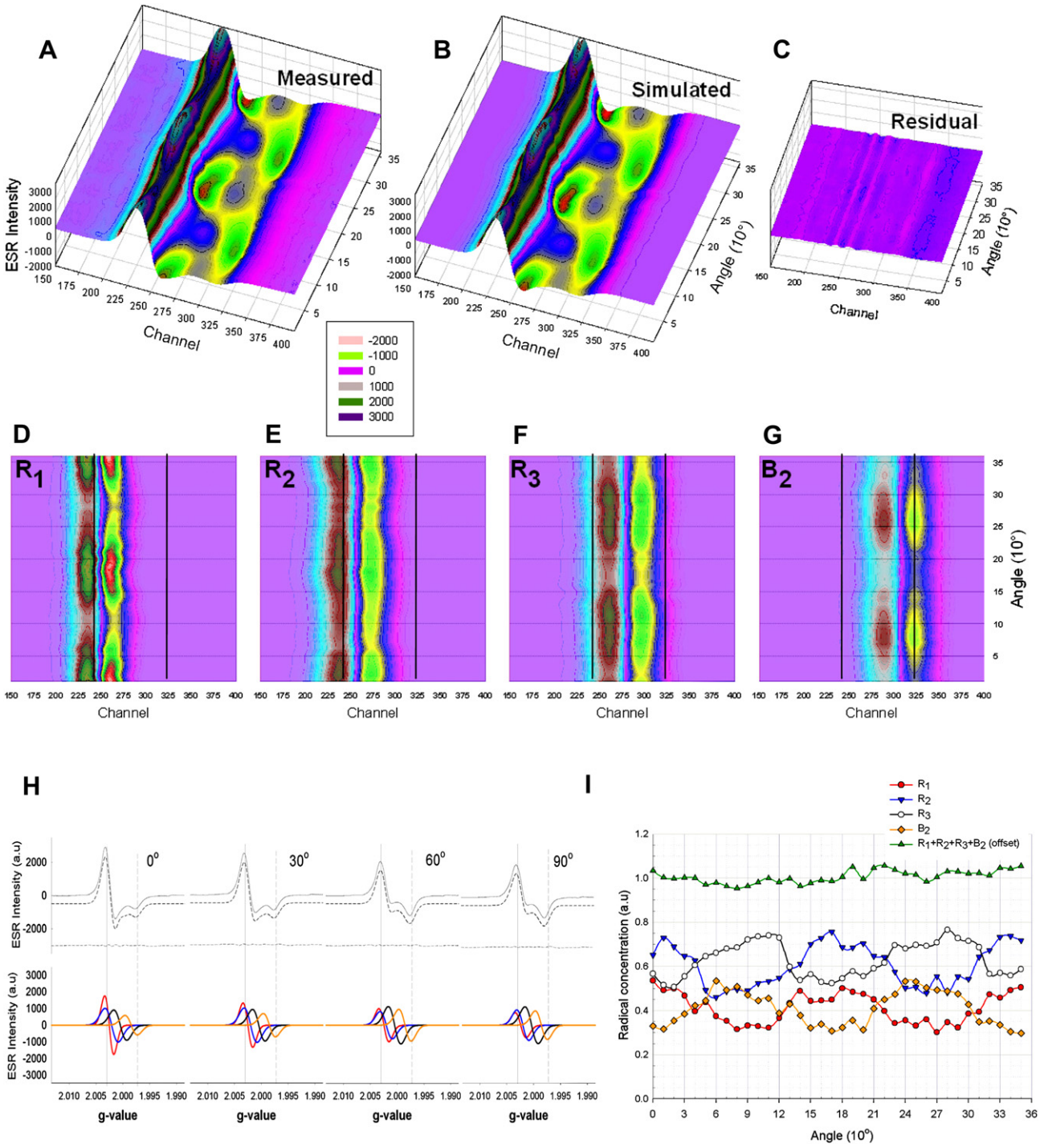

Fig. 6. Decomposition of the spectra in Y-configuration. For the description of the diagrams see Fig. 5.

R_1, R_2 and B_2 show a 180° symmetry, which is expected from an oriented CO_2^- component. In contrast, R_3 shows a pronounced 90° symmetry (Fig. 5I). While this is surprising, the stack of the measured spectra shows a widening of the T1–B1 peak with a 90° symmetry (arrows in Fig. 5A).

The sum of the radical concentrations of the four fitted components (Fig. 5I) shows some angular dependency (0.2). However, any other combination (i.e., excluding one the fitted components) would lead to larger angular variations. We therefore conclude that all fitted components are associated with CO_2^- radicals.

3.2.2. *Y-configuration*

The angular responses in the Y-configuration are rather similar to Z (Fig. 6). T1–B1 and B2 vary by 0.62 and 0.53, respectively. The differences between Y and Z for B_2 are smaller variations in width and *g*-value as well as a significantly smaller average intensity, R_2 shows a larger angular variation (0.49) and R_3 has a somewhat smaller average concentration and converts into a 180° symmetry. R_1 and R_2 show similar angular behaviours and their maxima and minima are offset by 90° from B_2. The angular response of R_3 is similar to B_2. The intensity variations in T1–B1 are caused in equal measures by the variations in R_1 and R_2. The

Please cite this article in press as: Joannes-Boyau, R., et al., Decomposition of the angular ESR spectra of fossil tooth enamel fragments, Radiation Measurements (2010), doi:10.1016/j.radmeas.2010.06.029

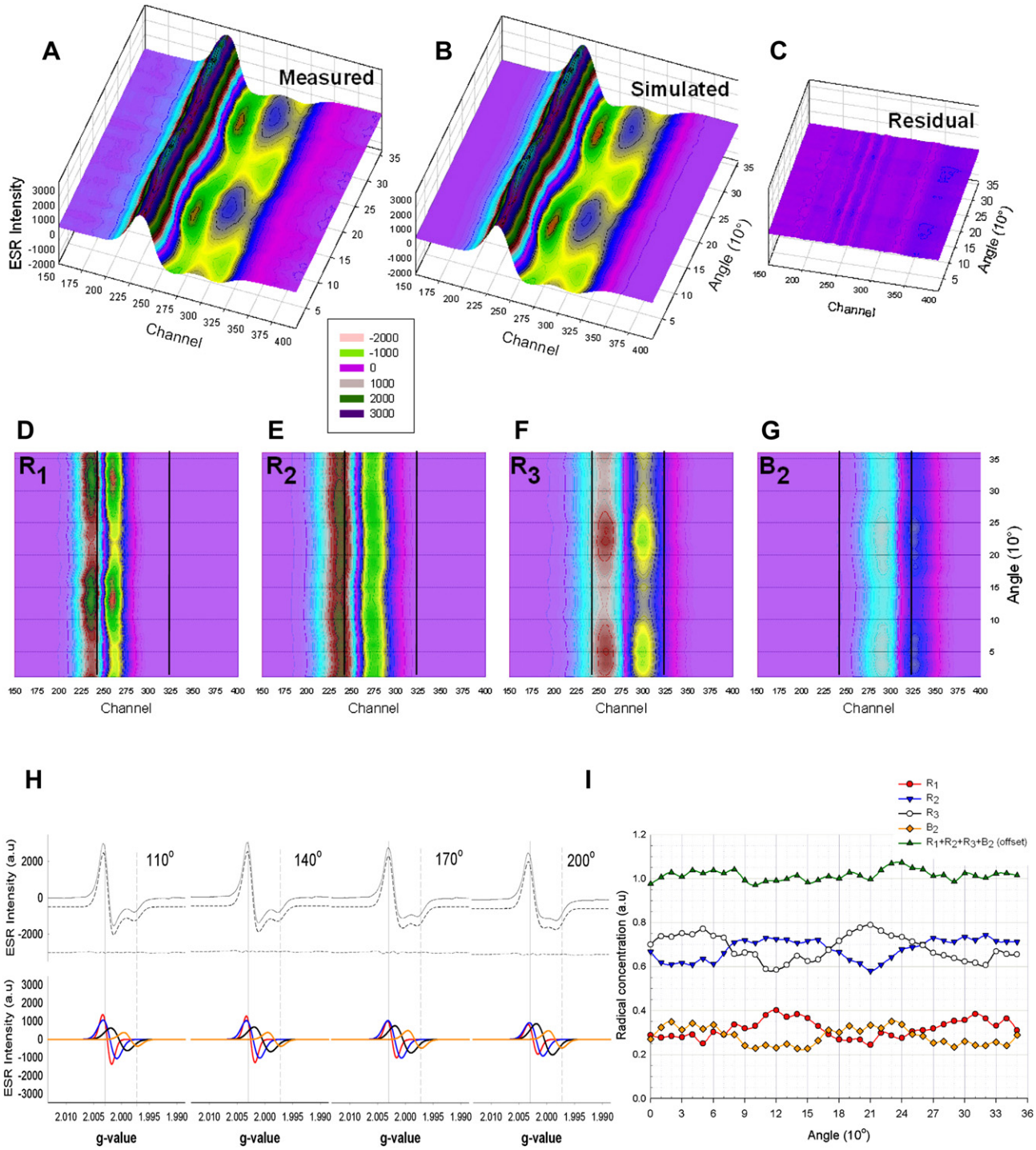

Fig. 7. Decomposition of the spectra in X-configuration. For the description of the diagrams see Fig. 5.

sum of the four fitted components shows a small angular dependency of 0.1.

3.2.3. X-configuration

The X-configuration shows the smallest angular variability in T1−B1 and B2 of 0.31 and 0.40, respectively (Fig. 7). R_1, R_2 and B_2 show the smallest variations in line widths and angular variations. R_2 has its largest intensity while R_1 and B_2 their smallest. R_3 has its largest line width. The variations in T1−B2 are caused in equal measure by R_1 and R_2 (the latter has a smaller angular variation, but much higher concentrations). As in the previous configurations, R_1 and R_2 show similar angular behaviours and their maxima and minima are offset by 90° from B_2 and R_3. The sum of the four fitted components shows a small angular dependency of 0.1.

It is perhaps noteworthy that any peak-to-peak measurements on powders for geochronology purposes or retrospective dosimetry should be carried out on T1-B2, as their interdependency minimises the angular variability of AICORs (see last column in Table 1). Nevertheless, further studies are required on dose reconstruction to be able to propose a clear statement on peak-to-peak measuring protocols.

Please cite this article in press as: Joannes-Boyau, R., et al., Decomposition of the angular ESR spectra of fossil tooth enamel fragments, Radiation Measurements (2010), doi:10.1016/j.radmeas.2010.06.029

Table 1
Angular variation of spectral features.

Configuration	T1–B1	B2	T1–B2
Z	0.60	0.74	0.25
Y	0.62	0.53	0.20
X	0.31	0.40	0.14

3.3. Uncertainties

In order to assess the uncertainties of our decomposition approach, we firstly ran our Monte Carlo simulation several times on the same spectra with different values of initial parameters (i.e. initial *g* and width values, seed of the random number generator). Relatively small differences were observed resulting from the robustness of the fitting strategy. Secondly, a simulation was carried out on a second fragment (H4) immediately adjacent to the fragment discussed in this paper (H5). The results are summarised in Table 3. In spite of using different moulds resulting in somewhat different measurements positions in the cavity, the simulation results on the three configurations are very comparable. The changes in minimum and maximum *g*-values and widths range between −0.0002 and +0.0001 (average ± 0.00004) and −0.03 and +0.03 mT (average ± 0.01 mT), respectively. The changes in *g*-values are virtually within measurement error, and the line width changes are well below 5%. Changes in the minimum and maximum radical concentrations as well as changes angular variation are significantly larger, reaching up to 36% (average 9%) and 46% (average 20%), respectively. These large changes in the intensity derived parameters are not entirely surprising, considering discontinuous nature of the radical concentration curves (Figs. 5I, 6I and 7I). More importantly, the average relative radical concentrations of R_1, R_2, R_3 and B_2 changed only to a maximum of 9%, with an average of 1.3%. The relative contributions of R_1:R_2 were 36:64 and 37:63 for H5 and H4, respectively. This is particularly remarkable as R_1 and R_2 completely overlap. Most previous decomposition approaches on X-band (e.g. Jonas, 1995; Grün, 1998; Vanhaelewyn et al., 2000a) could not resolve closely overlapping signals. Altogether, we consider our results as robust.

3.4. Discussion

From the roughly 90° offsets between R_1, R_2 maxima and minima from B_2, we conclude that R_1 and R_2 are AICOR components. Based on its *g*-values, B_2 is either $g_{\|}$ or g_y of axial or orthorhombic CO_2^- radicals, respectively, or a combination of both. Note that the *g*-value of $g_{\|}$ or g_y is measured at the position of the dip, around 1.9972 (as indicated Fig. 1) whilst the *g*-values for the B_2 component is the position of the zero-passing (maximum of the absorption line) with *g*-values around 1.9985. R_1 may represent g_x of orthorhombic and R_2 $g_{\perp}$ of axial CO_2^- radicals.

A question remains with respect to the nature of R_3. The fact that R_3 is needed for minimising the angular dependency of the sum of all fitted components points to anisotropic CO_2^- radicals. To recapitulate, enamel fragments are a partially ordered system with some preferential direction of the hydroxyapatite crystals, but there is also a significantly number of crystals in random orientation (Macho et al. 2003). What is seen in the measurements are the extreme values of the preferential directions (g_x and g_y, $g_{\perp}$ and $g_{\|}$) whilst the other orientations are lumped into R_3, see also Liidja (2001). These may arise from the misalignments of the preferential mineralogical axes with the *x*, *y*, and *z*-axes of the fragment, but also from misalignments of certain crystal domains with the preferential mineralogical axes. It is interesting to note that the fitted parameters of R_3, apart from its width in X-configuration, hardly change in the three configurations. Its average *g*-value of 2.0005 ± 0.0001 is indistinguishable from the average value of isotropic CO_2^- radicals in hydroxyapatite (see above).

If R_3 is the composite of all misalignments, it would consist of a semi-infinite series of Gaussian components between the T1 and B2 positions. If there is no spatial preference, R3 would basically present a Gaussian error function. While such a series is difficult to simulate, it can be approximated by a Gaussian line. However, if the misalignments are not randomly distributed (see Fig. 8B, below), the shape of R_3 may change with angle (see e.g. Fig. 9B, below) and its Gaussian approximation may create mathematical artefacts. Our decomposition approach does not allow an accurate assessment of the line shape of R_3. As a result, it cannot entirely be excluded that R_2 is part of misaligned crystal domains or an artefact of the assumption that R_3 has a Gaussian line shape.

Two previous observations on enamel fragments of this tooth support the existence of two oriented CO_2^- components. Firstly, heating experiments showed angular shifts of the T1–B1 maximum position by about 30° (Joannes-Boyau and Grün, 2009), which could be most readily explained by a transfer of orthorhombic to axial CO_2^- radicals. Secondly, we found that it is not possible to fit the irradiation spectra of fossil tooth enamel fragments with a linear combination of the spectra of the natural sample and isotropic CO_2^- radicals. This should be possible if only one oriented and one non-oriented type of CO_2^- radicals were

Table 2
Results of the decomposition of enamel fragment H5, using the SA protocol with a mix of four Gaussian lines.

	Minimum g-value		Maximum g-value		Minimum width (mT)		Maximum width (mT)		Minimum radical conc.		Maximum radical conc.		Angular variation	Average radical conc.
	Angle (°)		Angle (°)		Angle (°)		Angle (°)		Angle (°)		Angle (°)			
Z-configuration														
R1	2.0025	180	2.0027	230	0.28	330	0.36	100	0.31	100	0.54	340	0.56	0.40
R2	2.0020	290	2.0023	50	0.33	170	0.42	310	0.52	30	0.70	160	0.29	0.61
R3	2.0003	60	2.0006	160	0.38	80	0.44	190	0.59	150	0.86	190	0.39	0.70
B2	1.9981	230	1.9987	0	0.33	240	0.42	10	0.41	350	0.70	80	0.53	0.55
Y-configuration														
R1	2.0025	100	2.0028	340	0.28	170	0.35	280	0.30	80	0.54	360	0.57	0.41
R2	2.0020	120	2.0023	340	0.39	110	0.42	320	0.46	60	0.76	170	0.49	0.61
R3	2.0005	270	2.0006	120	0.39	130	0.45	310	0.51	20	0.77	280	0.41	0.63
B2	1.9985	350	1.9987	110	0.38	70	0.41	300	0.30	350	0.53	80	0.58	0.41
X-configuration														
R1	2.0025	20	2.0028	150	0.27	170	0.30	280	0.24	210	0.40	120	0.49	0.32
R2	2.0020	20	2.0023	320	0.41	110	0.42	320	0.58	210	0.74	320	0.24	0.68
R3	2.0005	130	2.0006	210	0.47	130	0.53	310	0.58	120	0.79	210	0.30	0.69
B2	1.9984	130	1.9987	40	0.40	70	0.42	300	0.23	100	0.35	230	0.44	0.28

Please cite this article in press as: Joannes-Boyau, R., et al., Decomposition of the angular ESR spectra of fossil tooth enamel fragments, Radiation Measurements (2010), doi:10.1016/j.radmeas.2010.06.029

Table 3
Results of the decomposition of enamel fragment H4, using the SA protocol with a mix of four Gaussian lines.

	Minimum g-value		Maximum g-value		Minimum width (mT)		Maximum width (mT)		Minimum radical conc.		Maximum radical conc.		Angular variation	Average radical conc.
	Angle (°)		Angle (°)		Angle (°)		Angle (°)		Angle (°)		Angle (°)			
Z-configuration														
R1	2.0025	190	2.0027	210	0.28	330	0.35	110	0.28	110	0.50	330	0.58	0.38
R2	2.0020	280	2.0024	60	0.36	190	0.42	300	0.50	50	0.65	180	0.26	0.58
R3	2.0003	80	2.0006	160	0.39	90	0.47	180	0.51	150	0.82	170	0.47	0.65
B2	1.9982	230	1.9987	10	0.33	230	0.42	0	0.43	350	0.65	80	0.41	0.54
Y-configuration														
R1	2.0026	80	2.0028	350	0.27	170	0.32	280	0.22	80	0.48	0	0.54	0.36
R2	2.0019	110	2.0023	350	0.38	110	0.42	320	0.42	60	0.66	170	0.41	0.57
R3	2.0004	270	2.0006	110	0.41	130	0.48	310	0.56	20	0.74	280	0.28	0.65
B2	1.9985	320	1.9988	100	0.36	70	0.42	300	0.30	340	0.52	80	0.54	0.40
X-configuration														
R1	2.0026	20	2.0028	150	0.27	150	0.31	260	0.22	210	0.39	120	0.43	0.29
R2	2.0020	20	2.0023	290	0.41	110	0.42	280	0.60	210	0.72	290	0.18	0.67
R3	2.0003	110	2.0006	200	0.47	130	0.54	300	0.62	120	0.77	210	0.22	0.69
B2	1.9984	130	1.9987	220	0.39	70	0.42	300	0.19	140	0.38	230	0.49	0.29

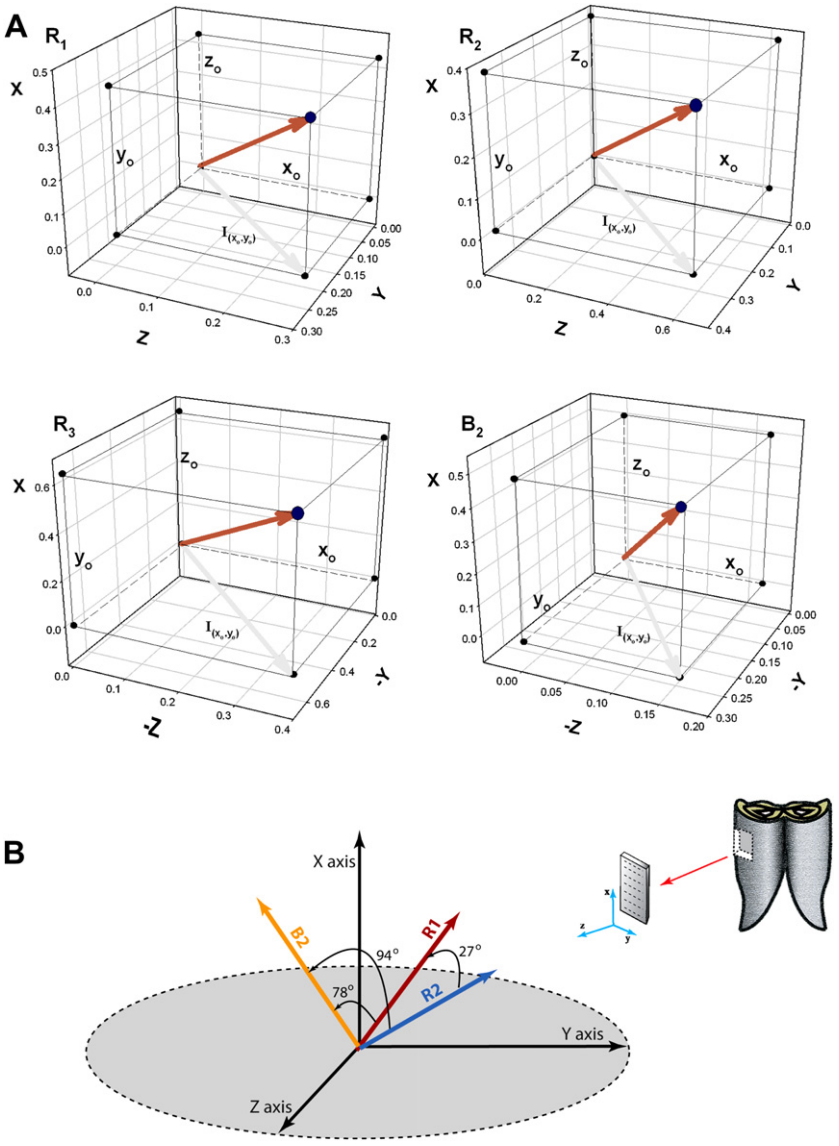

Fig. 8. A: The orientation of each radical has been estimated using the angular variation response. Each intensity maximum of each configuration corresponds to the strongest projection of the vector (reflecting the radical orientation and intensity) on the opposite plane parallel to the rotation plane. B: Directions of R_1, R_2, R_3 and B_2 with respect to the main axes of the fragment and their relative position (B). The grey circle corresponds to the plane perpendicular to the enamel/dentine junction.

Please cite this article in press as: Joannes-Boyau, R., et al., Decomposition of the angular ESR spectra of fossil tooth enamel fragments, Radiation Measurements (2010), doi:10.1016/j.radmeas.2010.06.029

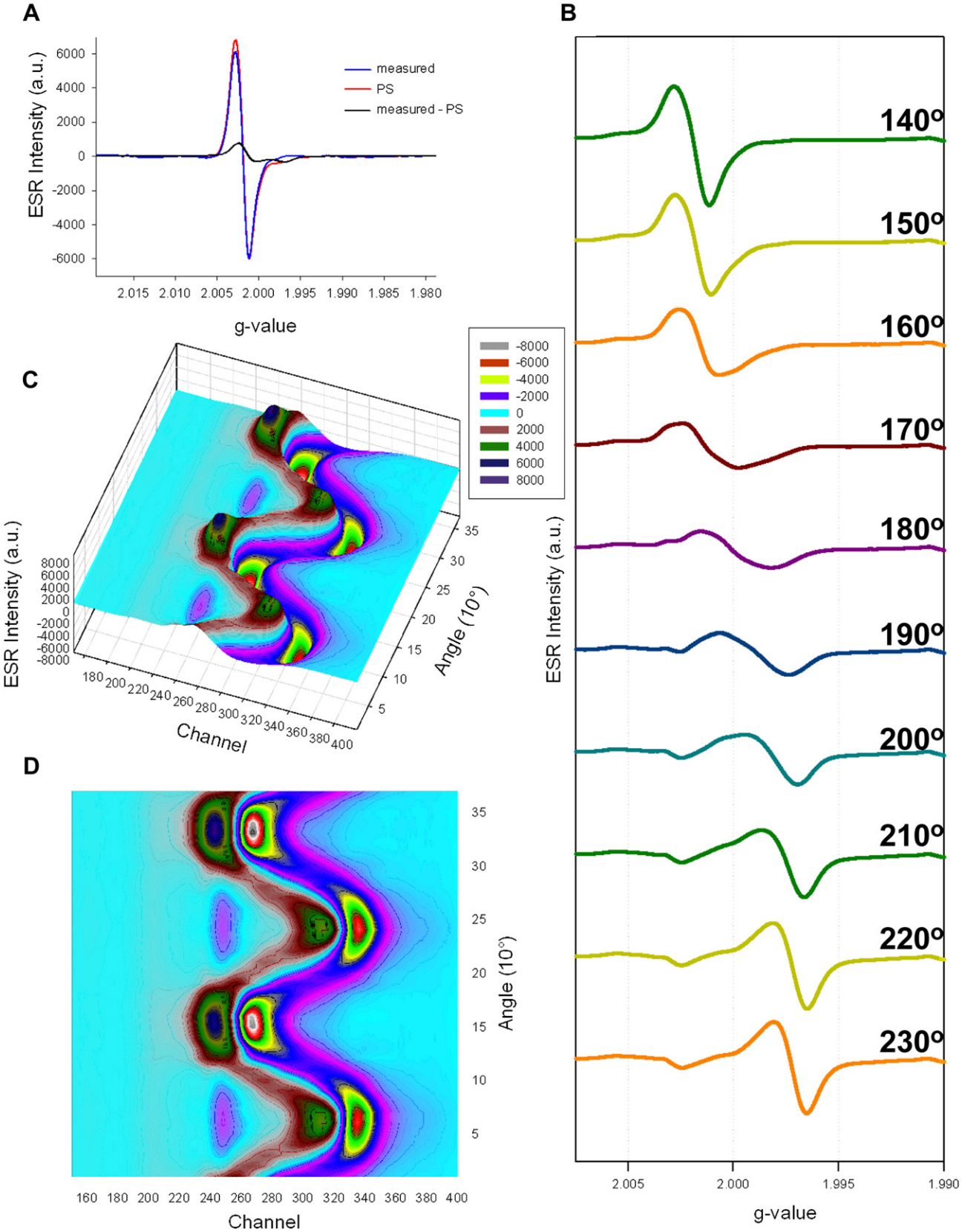

Fig. 9. Rotation of the fragment around an axis perpendicular to B_2 and the resultant of R_1 and R_2. A: Subtraction of the 9% powder spectrum in B2 minimum position. B: Rotation from T1–B1 maximum to the B2 maximum. C: 3D view of stacked spectra. D: map of intensities of stacked spectra.

Please cite this article in press as: Joannes-Boyau, R., et al., Decomposition of the angular ESR spectra of fossil tooth enamel fragments, Radiation Measurements (2010), doi:10.1016/j.radmeas.2010.06.029

present with different ratios in natural and irradiated spectra (Grün et al., 2008). The fits are particularly poor at intermediate angles between the T1–B1 and B2 minima and maxima.

Q-band studies on enamel powders found additional lines in the region of the $g = 2.0007$ (Jonas and Grün, 1997; Skinner et al., 2001), which can be attributed to tumbling CO_2^- radicals (see above). In addition, the intensity in the B2 position could not be fitted by a simulation of axial CO_2^- radicals (Jonas and Grün, 1997). Q-band studies on fragments of fossil tooth enamel clearly shows the presence of orthorhombic CO_2^- radicals (Bouchez et al., 1988; Rossi and Poupeau, 1990), which (i) had a somewhat different orientation to the axial CO_2^- radicals and (ii) were thermally less stable than the axial (and tumbling) CO_2^- radicals (Rossi and Poupeau, 1990). Taken all lines of evidence into consideration, we are confident that R_2 represents a component of orthorhombic CO_2^- radicals.

For the two fragments analysed, the ratio between R_1:R_2 is around 36:64. Thus far, we do not have any data for fossil tooth enamel. Vorona et al. (2006) found a relative distribution between axial and orthorhombic CO_2^- radicals in irradiated modern tooth enamel of approximately 20:75. They showed that orthorhombic CO_2^- radicals could convert into axial by heating. One would expect that the same happens over geological time scales of hundreds of thousands of years.

We can now use the measurements of the three configurations to calculate the main directions of the fitted components (Fig. 8A). Firstly, there is a clear separation between R_1 and R_2 of about 23° (Fig. 8B). This is very similar to the angular separation of 30° of CO_2^- components observed in previous heating experiments (Joannes-Boyau and Grün, 2009). The angle between R_1 and B_2 is 76° and between R_2 and B_2 98°. The angles are different from 90° because B_2 is a composite. The calculated angle between B_2 and the resultant vector of R_1 and R_2 is 86°. The direction of R_3 (Fig. 7A) is perhaps less meaningful, but may indicate a general preferential direction of the misaligned crystal domains.

Subsequent to these calculations, we inserted the enamel fragment into the goniometer so that it was rotated around the plane of the B_2 vector and the resultant vector of R_1 and R_2 (Fig. 9). After subtraction of a powder spectrum with 9% of the total radical concentration (Fig. 9A), we can clearly observe a behaviour that is closer to that described for single crystals (compare Figs. 3 and 9B). T1–B1 and B2 intensities can be virtually eliminated at 0° and 90°, respectively. However, in these two positions, the ESR spectrum cannot be fitted with a single Gaussian line, both require at least two components. This clearly indicates a large 'misalignment' component, as simulated by Liidja (2001), see his Fig. 13. At intermediate angles, a wider line occurs which resembles R_3 with a 90° symmetry, peaking between the T1–B1 and B2 maxima (compare to Fig. 5I). From these measurements we can also conclude that the maximum contribution of the NOCORs is 9%. This agrees well with a value of 10% derived from the annealing experiments on another fragment of this tooth (Grün et al., 2008).

We also tried to decompose this data set. The problem of R_3 not being of Gaussian line shape (particularly obvious between 170° and 200° in Fig. 9B) made it impossible to track R_1 and R_2 when their intensity decreased. Instead, R_3 was widening which then had a knock-on effect on the calculation of the line width of B_2. We are continuing to work on this problem.

At this stage it is not possible to deduct whether the R_1 and R_2 components are located in the same or different mineral domains, e.g. inside or on the surface of crystals with different sizes average crystal sizes etc… If orthorhombic CO_2^- radicals can be transferred into axial (as observed by Vorona et al., 2006) then these should be located in the same crystal domains.

4. Conclusions

We have developed a rapid method for the decomposition of the angular spectra of tooth enamel. The simulated annealing procedure seems particularly well suited to decompose overlapping signals, such as R_1 and R_2. All spectra can be satisfactory decomposed using four Gaussian Lines, R_1, R_2, R_3 and B_2. All fitted components seem related to anisotropic CO_2^- radicals. R_1 has been tentatively related to the g_x of orthorhombic and R_2 to $g_\perp$ of axial radicals. B_2 is a combination of g_y and $g_\parallel$ of the two anisotropic CO_2^- radicals. R_3 presents an envelope for misalignments, resulting from angles between the dominant axial directions and the principal axes of the fragment as well as misalignments of various crystal domains with the dominant axial directions. We found an angle of 23° between the directions of R_1 and R_2. The occurrence of two different anisotropic CO_2^- radicals in fossil tooth enamel is supported by Q-band studies on fossil enamel fragments (Bouchez et al., 1988; Rossi and Poupeau, 1990) and our earlier observations on the ESR response to heating (Joannes-Boyau and Grün, 2009) and that the irradiation spectra of irradiated fossil tooth enamel fragments cannot be fitted by a linear combination of the spectra of the natural sample and isotropic CO_2^- radicals.

Our decomposition approach will now allow the investigation of the irradiation effects in fossil tooth enamel and assess their relevance for dose response and dating.

Acknowledgments

We thank G. Liidja, Tallinn for providing us with one of his reprints that was difficult to obtain and N. Manson, Research School of Physical Sciences, ANU, for helpful comments. We are grateful to F. Callens and Henk Vrielinck, Gent, for their thorough advice in the earlier stages of this study. Aspects of this study were supported by ARC grant DP DP0664144 Microanalysis of human fossils: new insights into age, diet and migration.

References

Bouchez, R., Cox, R., Hervé, A., Lopez-Carranza, E., Ma, J.L., Piboule, M., Poupeau, G., Rey, P., 1988. Q-Band ESR studies of fossil teeth: consequences for ESR dating. Quaternary Science Reviews 7, 497–501.

Brik, A.B., Rosenfeld, L.G., Haskell, E.H., Kenner, G.H., Brik, V.B., 2000. Formation mechanism and localization places of CO_2^- radicals in tooth enamel. Mineralogie Journal (Kiev) 22, 57–67.

Brik, A.B., Shpak, A.P., Karbovsky, V.L., Kimenko, A.P., Dubok, V.A., Kalinichenko, A.M., Bagmut, N.N., Bevz, V.V., 2005. EPR of nanonized particles in biological and synthetic carbon containing apatites. Mineralogie Journal (Kiev) 27, 5–26.

Callens, F., Moens, P., Verbeeck, R., 1995. An EPR study of intact and powdered human tooth enamel dried at 400 °C. Calcified Tissue International 56, 543–548.

Callens, F., Vanhaelewyn, G., Matthys, P., Boesman, E., 1998. EPR of carbonate derived radicals: applications in dosimetry, dating and detection of irradiated food. Applied Magnetic Resonance 14, 235–254.

Callens, F.J., Verbeeck, R.M.H., Matthys, P.F.A., Martens, L.C., Boesman, E.R., 1987. The contribution of CO_3^{3-} and CO_2^- to the ESR spectrum near $g = 2$ of powdered human tooth enamel. Calcified Tissue International 41, 124–129.

Černý, V., 1985. A thermodynamical approach to the travelling salesman problem: an efficient simulation algorithm. Journal of Optimization Theory and Applications 45, 41–51.

Debuyst, R., Dejehet, F., Idrissi, S., 1993. Paramagnetic centers in γ-irradiated synthetic monohydrocalcite. Applied Radiation and Isotopes 44, 293–297.

Grün, R., 1998. Dose determination on fossil tooth enamel using spectrum deconvolution with Gaussian and Lorentzian peak shapes. Ancient TL 16, 51–55.

Grün, R., 2002. ESR dose estimation on fossil tooth enamel by fitting the natural spectrum into the irradiated spectrum. Radiation Measurements 35, 87–93.

Grün, R., 2006. Direct dating of human remains. Yearbook of Physical Anthropology 49, 2–48.

Grün, R., Joannes-Boyau, R., Stringer, C., 2008. Two types of CO_2^- radicals threaten the fundamentals of ESR dating of tooth enamel. Quaternary Geochronology 3, 150–172.

Ishchenko, S.S., Vorona, I.P., Okulov, S.M., Baran, N.P., 2002. ^{13}C hyperfine interactions of CO_2- in irradiated tooth enamel as studied by EPR. Applied Radiation and Isotopes 56, 815–819.

Joannes-Boyau, R., Grün, R., 2009. Thermal behavior of oriented and non-oriented CO_2^- radicals in tooth enamel. Radiation Measurements 44, 505–511.
Jonas, M., 1995. Spectral deconvolution of the ESR dating signal in fossil tooth enamel. Quaternary Science Reviews 14, 431–438.
Jonas, M., Grün, R., 1997. Q-band ESR studies of fossil tooth enamel: implications for spectrum deconvolution and dating. Radiation Measurements 27, 49–58.
Kirkpatrick, S., Gelatt, C.D., Vecchi, M.P., 1983. Optimization by simulated annealing. Science 220, 671–680.
Liidja, G., 2001. Electron paramagnetic resonance spectra of human tooth enamel with preferential oriented nanocrystals. Proceedings of the Estonian Academy of Sciences Physics and Mathematics 50, 227–246.
Macho, G.A., Jiang, Y., Spears, I.R., 2003. Enamel micro structure – a truly three-dimensional structure. Journal of Human Evolution 45, 81–90.
Metropolis, N., Rosenbluth, A.W., Rosenbluth, M.N., Teller, A.H., Teller, E., 1953. Equations of state calculations by fast computing machines. Journal of Chemical Physics 21, 1087–1092.
Mosegaard, K., Sambridge, M., 2002. Monte Carlo analysis of inverse problems. Inverse Problems 18, 79161–79162.
Porat, N., Zhou, L.P., Chazan, M., Noy, T., Horwitz, L.K., 1999. Dating the lower Paleolithic open-air site of Holon, Israel by luminescence and ESR technologies. Quaternary Research 51, 328–341.
Rossi, A.M., Poupeau, G., 1990. Radiation damage in bioapatites: the ESR spectrum of of irradiated enamel revisited. Radiation Measurements 17, 537–545.
Rudko, V.V., Vorona, I.P., Baran, N.P., Ishchenko, S.S., 2007. Gamma- and UV-induced CO_2^- radicals in tooth enamel. Radiation Measurements 42, 1181–1184.
Schramm, D.U., Rossi, A.M., 2000. Electron spin resonance (ESR) studies of CO_2^- radicals in irradiated A and B-type carbonate-containing apatites. Applied Radiation and Isotopes 52, 1085–1091.
Skinner, A.R., Chasteen, N.D., Shao, J., Blackwell, B.A.B., 2001. Q-band studies of the ESR signal in tooth enamel. Quaternary Science Reviews 20, 1027–1030.
Stoll, S., Schweiger, A., 2006. EasySpin, a comprehensive software package for spectral simulation and analysis in EPR. Journal of Magnetic Resonance 178, 42–55.
Stoll, S., Schweiger, A., 2007. EasySpin: simulating cw ESR spectra. Biological Magnetic Resonance 27, 299–321.
Vanhaelewyn, G., Callens, F., Grün, R., 2000a. EPR spectrum deconvolution and dose assessment of fossil tooth enamel using maximum likelihood common factor analysis. Applied Radiation and Isotopes 52, 1317–1326.
Vanhaelewyn, G.C.A.M., Morent, R.A., Callens, F.J., Matthys, P.F.A.E., 2000b. X- and Q-band electron paramagnetic resonance of CO_2^- in hydroxyapatite single crystals. Radiation Research 154, 467–472.
Vorona, I.P., Ishchenko, S.S., Baran, N.P., 2005. The effect of thermal treatment on radiation-induced EPR signals in tooth enamel. Radiation Measurements 39, 137–141.
Vorona, I.P., Ishchenko, S.S., Baran, N.P., Petrenko, T.L., Rudko, V.V., 2006. Evidence of annealing-induced transformation of CO_2^- radicals in irradiated tooth enamel. Radiation Measurements 41, 577–581.
Vugman, N.V., Rossi, A.M., Rigby, S.E.J., 1995. EPR dating CO_2^- sites in tooth enamel apatites by ENDOR and triple resonance. Applied Radiation and Isotopes 46, 311–315.

Please cite this article in press as: Joannes-Boyau, R., et al., Decomposition of the angular ESR spectra of fossil tooth enamel fragments, Radiation Measurements (2010), doi:10.1016/j.radmeas.2010.06.029